INDIAN JOURNAL OF SCIENCE AND TECHNOLOGY

RESEARCH ARTICLE

# Structural and Optical Properties of Hydrothermally Synthesized $Co_{0.3}Zn_{0.7}Al_xFe_{2-x}O_4$ (x = 0.2 – 0.8) Nanoparticles

**G Pakardin[1]*, D Chinna Venkata Subbaiah[2], S Dastagiri[3]*, Kongi Prasad[2], G Lokeswara Reddy[4], M V Lakshmaiah[3], M Sree Latha[5]**

**1** Department of Physics, SCNR Govt. Degree College, Proddatur, 516360, YSR Kadapa, A.P, India
**2** Department of Physics, Yogi Vemana University, YSR Kadapa, 516005, A.P, India
**3** Department of Physics, Sri Krishnadevaraya University, Anantapuramu, 515003, A.P, India
**4** Department of Physics, Govt. Degree College, Yerraguntla, 516309, YSR Kadapa, A.P, India
**5** Department of Science and Humanities, Matrusri Engineering College, Saidabad, 500059, Hyderabad

OPEN ACCESS

**Received:** 23-11-2024
**Accepted:** 19-12-2024
**Published:** 11-01-2025

**Citation:** Pakardin G, Subbaiah DCV, Dastagiri S, Prasad K, Reddy GL, Lakshmaiah MV, Sree Latha M (2025) Structural and Optical Properties of Hydrothermally Synthesized $Co_{0.3}Zn_{0.7}Al_xFe_{2-x}O_4$ (x = 0.2 – 0.8) Nanoparticles. Indian Journal of Science and Technology 18(1): 51-58. https://doi.org/10.17485/IJST/v18i1.3822

* **Corresponding authors**.

pakarags@gmail.com

drsdg2020@gmail.com

**Funding:** None

**Competing Interests:** None



Published By Indian Society for Education and Environment (iSee)

**ISSN**
Print: 0974-6846
Electronic: 0974-5645

## Abstract

**Objectives**: Investigations on structural and optical studies of $Co_{0.3}Zn_{0.7}Al_xFe_{2-x}O_4$ (x = 0.2 – 0.8)/CZAFO nanoparticles synthesized through hydrothermal method are presented in this paper. **Methods:** $Co_{0.3}Zn_{0.7}Al_xFe_{2-x}O_4$ (x = 0.2 – 0.8) samples are synthesized by hydrothermal method. Structural and Optical characterization of the samples is done by using X-ray diffraction (XRD), photoluminescence (PL), UV-Vis spectrophotometer and Fourier transform infrared spectroscopy (FTIR). **Findings:** The spinel cubic structure is established with the X-Ray Diffraction pattern. The crystallite size values range from 5.610 to 6.188 nm increasing with substitution $Al^{3+}$ concentration x, according to the Debye-Scherer formula. Photoluminescence emission between 360 nm and 615 nm exposes the radiative deficiencies and oxygen vacancies by the effect of $Al^{3+}$ substituting CZFO nanoparticles at room temperature. FT-IR confirms the existence of metal oxides. Using the UV-visible spectrophotometer and the impact of $Al^{3+}$ substitutions on Co-Zn ferrite nanoparticles, optical energy band gap in the samples was investigated. Samples' energy band gap decreases as the $Al^{3+}$ content rises, from x = 0.2 to 0.8. **Novelty**: Investigations on the effect of Al substitution on structural and Optical properties of $Co_{0.3}Zn_{0.7}Al_xFe_{2-x}O_4$ nanoparticles were optical band gap energies ranging from 1.647 eV to 1.487 eV, depending on the composition (x = 0.2, 0.4, 0.6, and 0.8), hold promise for sort of optoelectronic applications and including photocatalysis, optical sensors and biomedical imaging. Also, optical band gap energy ($E_g$) values were provided to indicate the semiconductor nature of CZAFO nanoparticles.

**Keywords:** Aluminum; Nanoparticles; Hydrothermal Method; Optical Property; Cobalt-Zinc ferrite (CZFO)

## 1 Introduction

Nanoparticles of spinel ferrites have been gaining noteworthy consideration in current years owing to their unique electrical, magnetic and catalytic properties, which render them promising candidates for a wide range of applications including microwave devices, catalysis, magnetic recording media, electromagnetic interference shielding, biomedical applications, etc. Incorporation of aluminum (Al) into the $CoZnFe_2O_4$ lattice has been reported to significantly influence its magnetic and structural properties. Aluminum substitution is known to induce changes in the cations distribution and lattice parameters, thereby affecting the magnetic behavior and electrical conductivity of the ferrite nanoparticles. Additionally, Al-substituted spinel ferrites have shown enhanced catalytic activity in various chemical reactions due to the modification of surface properties and the formation of active sites [1,2].

The standard chemical formula of spinel ferrites is $MFe_2O_4$, where M represents a divalent transition metal (M = divalent metal ions; examples include Mg, Zn, Ni, Co, etc.) or an appropriate combination of these ions. The mineral spinel is a naturally occurring mineral. A strongly packed oxygen crystal collection, with thirty two oxygen ions for each unit cell (the smallest unit recurring in the crystal system), is a part of the makeup of the spinal lattice. Two forms of spacing between anions remain in the face-centered cubic (FCC) layout as a result of the packing of these anions. The two types of spacing are depicted as tetrahedrally matched sites (A), circumscribed through 4 neighboring oxygen atoms, and octahedrally matched sites (B), circumscribed through 6 neighboring oxygen atoms [3]. There are 32 octahedral and 64 tetrahedral sites altogether in the unit cell. However, only eight tetrahedral sites and sixteen octahedral sites are engaged, neutral of the leaving structure electrically [2,3]. Spinel ferrite powders at the nanoscale are produced using a variety of techniques, such as mechanical milling, sol-gel, reverse micelle, citrate–gel and microemulsion [1–5].

The study, Structural and Optical Properties of Nickel-Doped Zinc Sulphide Nanomaterials, demonstrates how Ni doping can effectively tune the properties of ZnS nanoparticles, making them promising candidates for applications in photocatalysis, optoelectronics, and other fields requiring specific optical and electrical properties. Further research could concentrate on optimising the Ni doping level to increase the required characteristics for the targeted applications [6].

Regarding the structural, electrical, and magnetic properties of $Co_{0.3}Zn_{0.7}Al_xFe_{2-x}O_4$ (x = 0.2, 0.4, 0.6, 0.8) synthesized by hydrothermal technique, no systematic research has been published in the literature. While distinct investigations focus on the magnetic and structural characteristics of $Co_{1-x}Zn_xFe_2O_4$ [4] ferrite system are using the hydrothermal technique, the doped Zn/Al on cobalt ferrites remain unexplored.

Particular focus has recently been on the diamagnetic substitution in mixed ferrites. The role of substituents in revolutionizing the physical uniqueness of basic ferrites and the process that leads to enhanced magnetic awareness has not been extensively researched. It is extremely complicated to fabricate ferrite materials with high superiority, economical and squat loss by the side of power applications for high frequency. To acquire new behavior of ferrites on the nanoscale, in this aspect we have selected $Al^{3+}$ substitution on Co-Zn ferrites with a composition of $Co_{0.3}Zn_{0.7}Al_xFe_{2-x}O_4$ (x = 0.2, 0.4, 0.6, 0.8)/ CZAFO nanoparticles for structural and functional properties.

## 2 Methodology

We choose cobalt nitrate [$Co(NO_3)_2{\cdot}6H_2O$ (99.8% purity, Sigma-Aldrich)], Zinc nitrate [$Zn(NO_3)_2{\cdot}6H_2O$ (99.8% purity, Sigma-Aldrich)], Aluminum Nitrate nonhydrate [Al $(NO_3)_3{\cdot}9H_2O$ (99.8% purity, Sigma-Aldrich)] and ferric nitrate [$Fe(NO_3)_3{\cdot}9H_2O$ (99.9% purity, Sigma-Aldrich)] as the starting materials for the synthesis of $Co_{0.3}Zn_{0.7}Al_xFe_{2-x}O_4$ (x = 0.2, 0.4, 0.6, 0.8) nanoparticles. In hydrothermal reaction, an aqueous solution of sodium hydroxide (NaOH) pellets was also employed as the solvent.

The initial synthesis of $Co_{0.3}Zn_{0.7}Al_xFe_{2-x}O_4$ (x = 0.2, 0.4, 0.6, 0.8) / CZAFO nanoparticles followed the stoichiometric equation. The raw ingredients (in nitrate form) were combined in a brand-new glass beaker after being weighed on a digitally sensitive balance using this stoichiometric procedure. Subsequently, the nitrate components were dissolved in distilled water in a glass beaker. Next, a magnetic stirrer set at 430 rpm was used to stir the combined solution. The nitrate solution was gradually supplemented with drops of the NaOH aqueous solution during this interim. The solution turned white and tasted good after being stirred for two hours. This mixture solution was then transferred to a 500 ml Teflon bowl and stored in an autoclave made of stainless steel. Subsequently, the autoclave's screws were tightened to avoid a solution explosion during the hydrothermal reaction. After that, a programmed hot air oven was used to store the autoclave. The hydrothermal reaction took place in the oven at 160°C for eight hours. Once the process was finished, the hot-air oven was cooled to room temperature. The sample was taken out of the Teflon bowl and cleaned ten or twelve times more till the pH reached seven in the following stage. The powder sample was then dried out for two hours at 60 °C in a hot air oven. For fifteen minutes, the dry $Co_{0.3}Zn_{0.7}Al_xFe_{2-x}O_4$ (x = 0.2, 0.4, 0.6, 0.8)/CZAFO nanopowder was grinding an agate mortar to produce uniform powder particles as shown in Figure 1.

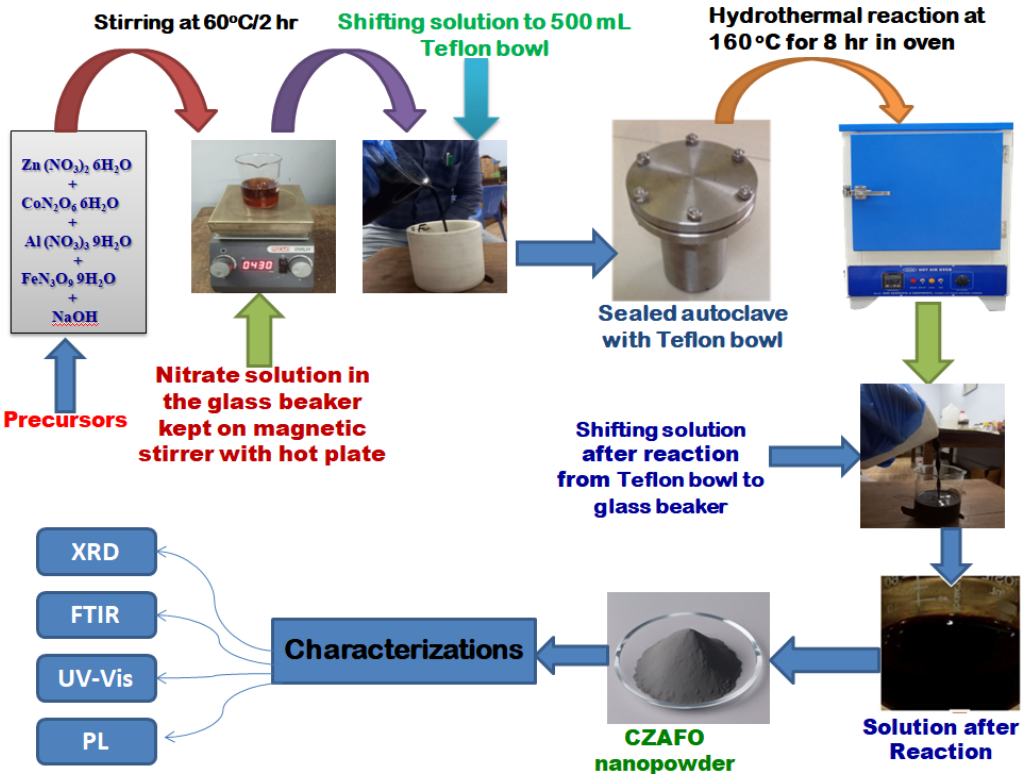


**Fig 1. The synthesis process of CZAFO nanoparticles**

## 3 Results and Discussions

### a. X-ray diffraction analysis

All of the observed peaks were indexed to the 220, 311, 440, 422, 511, and 440 planes of the spinel lattice and a well-crystallized structure devoid of any other phases was discovered; according to XRD pattern of the samples, which is displayed in Figure 2. Every composition's XRD pattern may be classified as a pure cubic spinel structure when compared to JCPDS data. Every peak on the XRD corresponds to the JCPDS file number 22-1086. The tiny half-width of each peak revealed the enormous crystallite size. The lattice constant intended for every peak of every sample was determined via the XRD data and the formula a= d $(h^2+k^2+l^2)^{1/2}$, where h, k, and l are the Miller indices of crystal planes. Figure 2 illustrates how the increase in $Al^{3+}$ concentration from 0.2 to 0.8 causes the lattice parameter (a) to increase from 8.210 to 8.322 Å. It is demonstrated with the intention of lattice parameter increases linearly by way of raise in $Al^{3+}$ concentration, suggesting lattice expansion since $Al^{3+}$ has smaller ionic radius (0.051 nm) than $Fe^{3+}$ (0.064 nm). Thus, the spinel cubic unit cell's unit cell volume ($V = a^3$) increased from 553.387 to 576.345 $Å^3$. Here, Shannon ionic radii data and the likely cation distribution help us understand how lattice constants vary. Due to iron's higher ionic radius than that of aluminum, if $Al^{3+}$ cations were added to Co-Zn ferrite, there may be a chance for it to occupy the $Fe^{+3}$ sites[7,8]. The unit cell will therefore contract, which may cause the unit cell's dimensions and volume to increase. The Scherrer equation for X-ray diffraction (XRD) peaks enabled us to achieve an average crystallite size[9,10]: $D_{ave} = 0.9\lambda/\beta \, Cos\Theta$ where $D_{ave}$ is the average crystallite size (nm), $\lambda$ is the wavelength of incident X-ray beam (0.15406 nm), $\beta$ is the full-width half maxima (FWHM) and $\Theta$ is Bragg's angle. The average crystallite size was determined to be in 5.610 - 6.188 nm range and was found to be very small. The concentration of $Al^{3+}$ substituting is increased, resulting in crystallites growing in size from 5.610 nm (x = 0.2) to 6.188 (x = 0.8). The rising $Al^{3+}$ content was found to slightly increase the lattice parameters, crystallite size and volume of the nanoparticles, indicating lattice expansion because of Aluminumsmaller ionic radii. The strain and FWHM showing a decreasing trend with increasing $Al^{3+}$ concentration (x=0.2-0.8) indicated a decrease in lattice distortion and crystalline defect. The $\rho_x$ was estimated through the help of the standard relations $\rho_x = Z\,Mw/Na^3$ for

cubic structure, where 'Mw' is the molecular weight of the composition (see Table 1), 'N' is Avogadro's number ($6.023 \times 10^{23}$) and 'a' is the lattice parameter. According to the obtained data, the density dropped from 5.601 to 4.978 gram per $cm^3$. Moreover, the dislocation density ($\rho$) is calculated by using the formula: $\rho = 1/D^2$, where D is the average crystallite size. Dislocation density values decreased from 3.177E+16 to 2.611E+16 $m^{-2}$ when $Al^{3+}$ concentrations increased by x= 0.2 -0.8. To conclude, specific surface area (S) the entire samples were established with the formula: $S = 6000/(D^*\rho_x)$, where symbols have their usual meaning. The 'S' was increased from 190.951 to 194.780 $m^2\ g^{-1}$ for x = 0.2 – 0.8 contents [11–14].

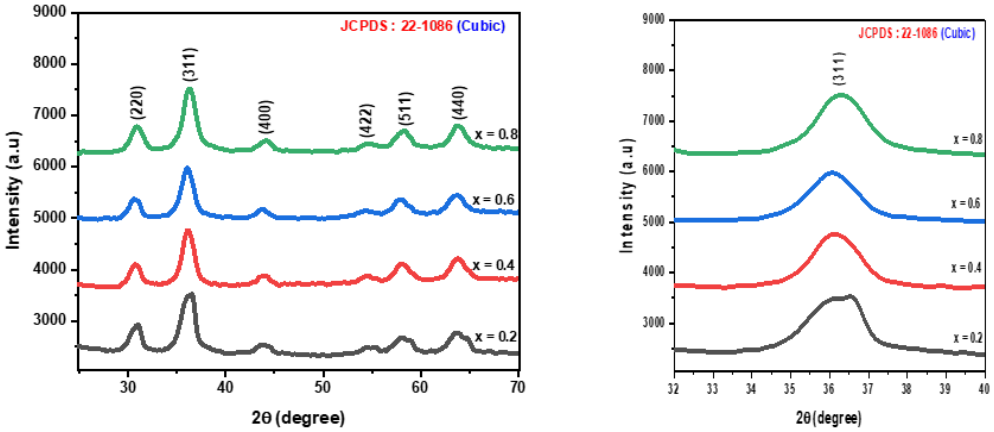


**Fig 2. XRD patterns of CZAFO nanoparticles**

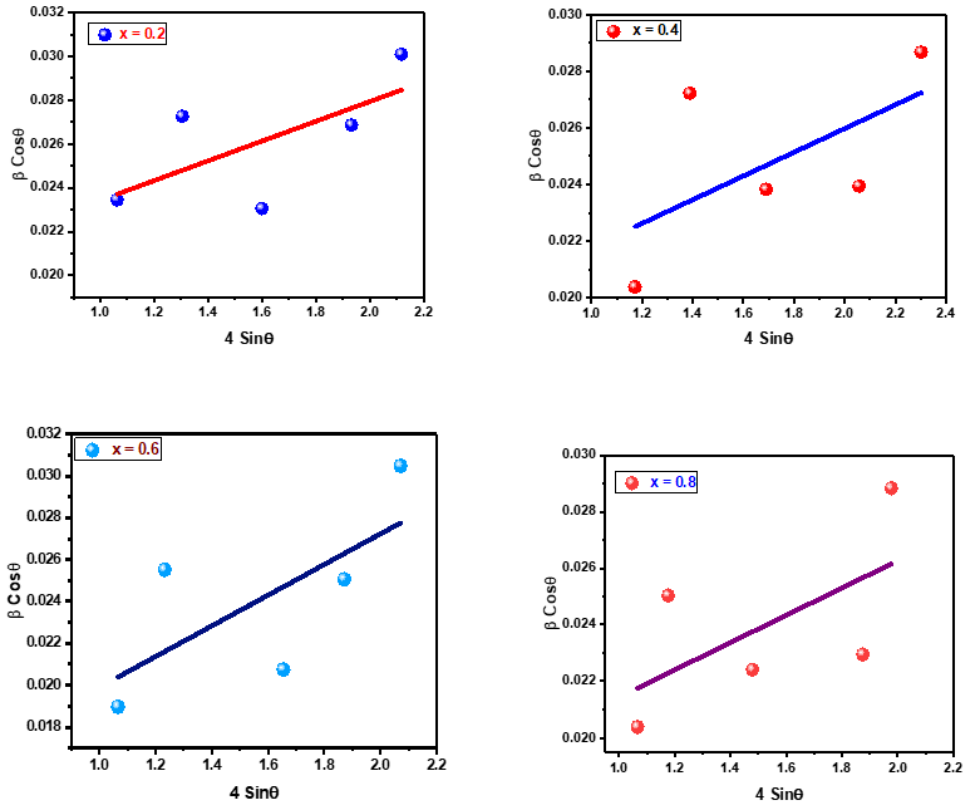


**Fig 3. W-H plots of CZAFO nanoparticles**

**Table 1. Data on structural and physical parameters of CZAFO nanoparticles**

| Parameters | x=0.2 | x=0.4 | x=0.6 | x=0.8 |
|---|---|---|---|---|
| **a (A°)** | 8.210 | 8.238 | 8.249 | 8.322 |
| **$D_{ave}$ (nm)** | 5.610 | 5.805 | 5.915 | 6.188 |
| $\varepsilon$ | 0.0169 | 0.0162 | 0.0158 | 0.0151 |
| $\beta$ **(rad)** | 0.0279 | 0.0277 | 0.0263 | 0.0262 |
| **V ($A^{\circ 3}$ )** | 553.387 | 559.068 | 561.311 | 576.345 |
| **MW (g/mol)** | 233.36 | 227.59 | 221.81 | 216.04 |
| $\rho_x$ **(g/$cm^3$ )** | 5.601 | 5.407 | 5.248 | 4.978 |
| **S ($m^2$ /g)** | 190.951 | 191.158 | 193.287 | 194.780 |
| $\rho$**($m^{-2}$ )** | 3.177E+16 | 2.967E+16 | 2.858E+16 | 2.611E+16 |
| **D** $_{W-H}$ | 7.329 | 7.879 | 7.942 | 8.324 |
| $\varepsilon_{W-H}$ | 0.0045 | 0.0041 | 0.0046 | 0.0048 |

The Williamson – Hall (W – H) plots (in Figure 3) are a widely used schematic tool for micro-strain ($\varepsilon_{W-H}$) and average crystallite size ($D_{W-H}$) estimation. The W-H plots between $\beta Cos\theta$ versus $4Sin\theta$ in the current study were created utilizing linearly compatible relationships: $B\ Cos\Theta = \frac{K\lambda}{D} + 4\varepsilon Sin\Theta$, where $\lambda$ is the wavelength, $\beta$ is Full-Width Half Maxima (FWHM), $\Theta$ is Bragg's diffraction angle, $\varepsilon$ is Micro-strain and D is crystallite size. Where the intercept value is connected with the size of the crystallites ($D_{W-H}$) and the slope of a straight line is related to the micro-strain ($\varepsilon_{W-H}$). Table 1 lists $\varepsilon_{W-H}$ and $D_{W-H}$ resultant values. The values obtained from the W-H plots using the Scherrer theorem and values $\varepsilon_{W-H}$ & $D_{W-H}$ are finally determined weren't in good agreement. $D_{W-H}$ increased as composition shifted from x=0.2 to 0.8, and $\varepsilon_{W-H}$ increased as composition shifted from both started to decline at x=0.4 [11,12,15].

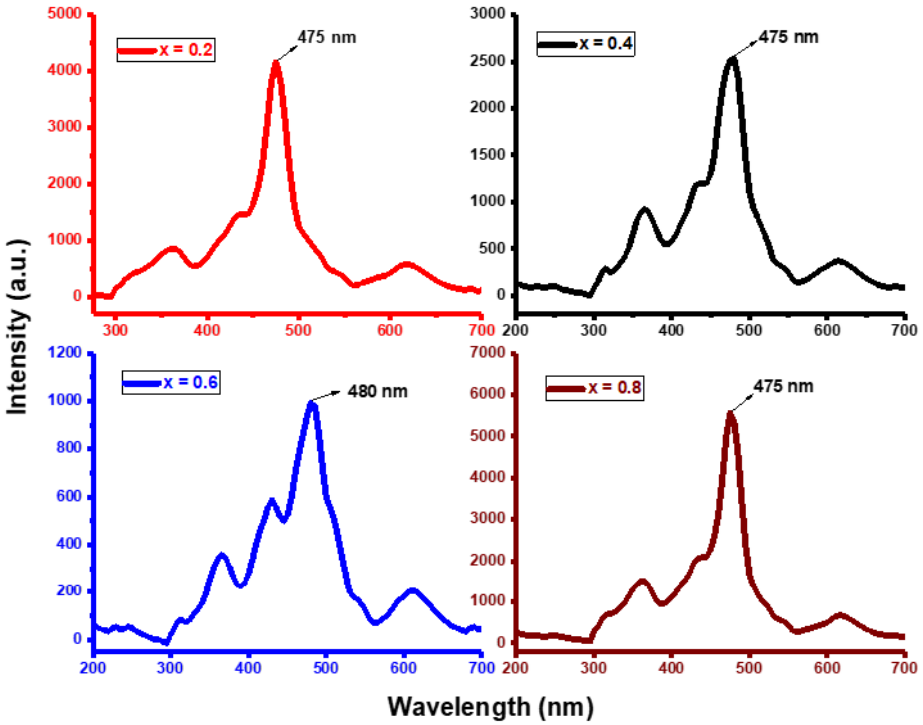


**Fig 4. PL spectra of CZAFO nanoparticles**

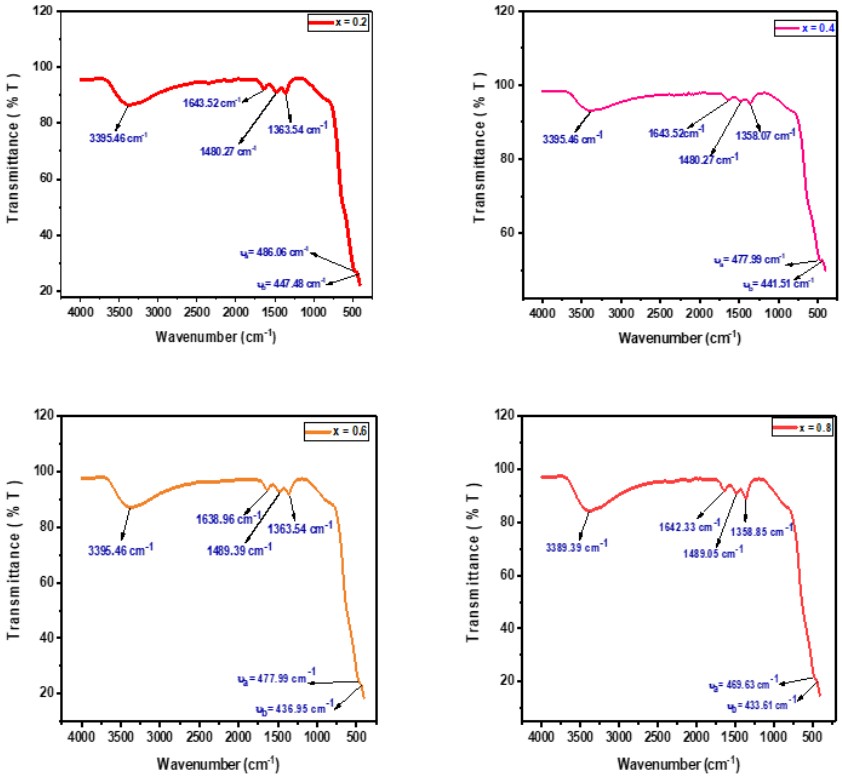


**Fig 5. FT-IR spectra of CZAFO nanoparticles**

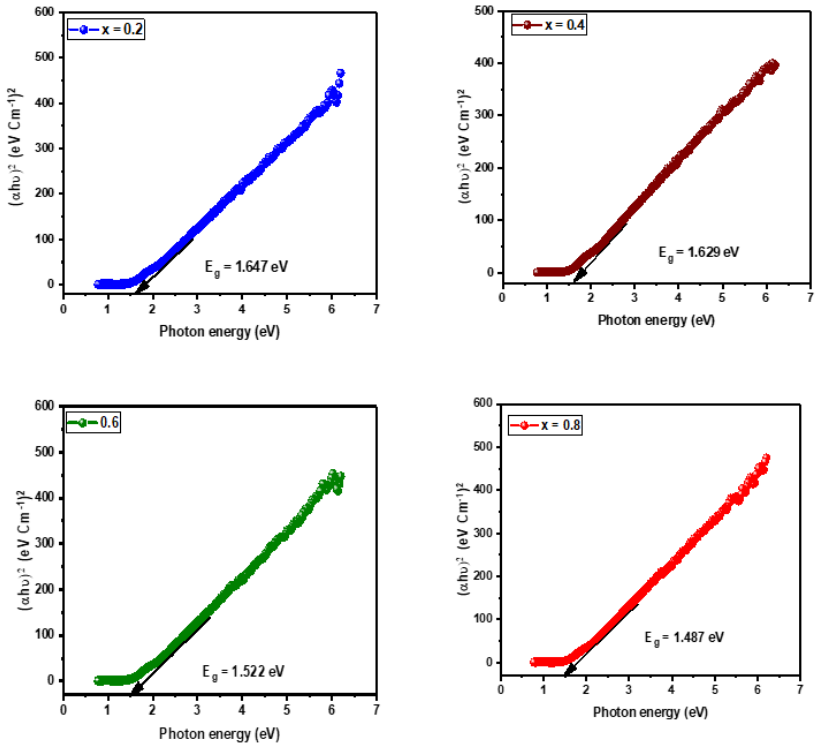


**Fig 6. Photon energy ($h\upsilon$) versus $(\alpha h\upsilon)^2$ plots of CZAFO nanoparticles**

### b. Photoluminescence properties

The effect of $Al^{3+}$ substituted CZFO nanoparticles on the photoluminescence property was investigated using PL spectra at room temperature and an excitation wavelength of 300 nm. The PL spectra of samples are represented in Figure 4. The visible range between 360 and 615 nm was where the emission peaks were observed, with a maximum observed at 475 nm for x = 0.2, 0.4 & 0.8 and 480 nm for x = 0.6. The radiative deficiencies at grain borders [12,13] and the oxygen vacancies inside the crystal structure [13] could be the cause of this electronic emission. Here, we have shown that an increase in $Al^{3+}$ ions leads to stronger and widely spaced peaks. The figure illustrates how peak positions vary in intensity but stay almost constant. It is known that for x = 0.2, a drop in crystallite size measured in nm, has been recorded. The radiative defects that are present close to the valence band of content x = 0.8 may be the cause of the shift in PL intensity peaks towards higher wavelengths. An earlier study has described the phenomenon of a transfer mechanism between iron (octahedral sites) and the surrounding oxygen anion in the spinel ferrites. Luminescence behavior of $CoFe_2O_4$ may result from intra-band gap defects (oxygen vacancies) and spinel-type structures, which both carry this charge transfer process [13]. Our research's results are in good accord with previous studies on the spinel ferrites [12,13]. However, given the setting of $Al^{3+}$ substitution $Co_{0.3}Zn_{0.7}Al_xFe_{2-x}O_4$ (x = 0.2–0.8) nanoparticles, it could be considered an honorable discovery to discover such a broad visible spectrum. Thus, the produced materials might be a good fit for optical device applications.

### c. FTIR analysis

The Fourier transform infrared spectra (FTIR) of CZAFO nanoparticles were recorded over the 4500–400 $cm^{-1}$ wave number range as shown in Figure 5. We detected absorption bands in the current samples' FTIR spectra at two distinct locations. The ranges in which the $\upsilon_a$ and $\upsilon_b$ peaks were observed were 469 to 486 $cm^{-1}$ and 434 to 447 $cm^{-1}$, respectively. The creation of the $\upsilon_a$ and $\upsilon_b$ absorption bands demonstrated the presence of metal oxide stretching vibrations. Fe-O may be indicated by the $\upsilon_a$ band location. Conversely, metal oxide bonds of Co-O, Zn-O, and Al-O can be found at the $\upsilon_b$ band location. It is known that the Fe-O bond can be reflected by the '$\upsilon_a$' inside the overall spinel ferrite structure ($MFe_2O_4$). In the same way, the M-O bonds can be provided by the "$\upsilon_b$" [8,9]. It appears that this investigation verified the formation of the cubic spinel structure of CZAFO nanoparticles. Additionally, as the XRD study discusses, the addition of $Al^{3+}$ to the CZFO system can produce a greater amount of Feions. By looking at the location of the Fe-O vibrations on both sides, the FTIR spectra provided proof of this. Numerous tiny subsidiaries a peak positions were observed in the vicinity of Fe-O. The existence of Feions may be indicated by these subsidiaries peaks. According to reports in the literature [11,16], this was regarded as a Jahn-Teller distortion. Additionally, a few band locations were observed at 3389 to 3395 $cm^{-1}$, 1480 to 1489 $cm^{-1}$ & 1358 to 1363 $cm^{-1}$. These positions developed as a result of stretching vibrations that were appropriate for the O-H bonds and $H_2O$ molecule contortion [11,16,17].

### d. UV-Visible Spectrum Analysis

UV–visible spectrophotometer is an essential tool to scrupulously observe the optical energy gaps of nanoparticles. CZAFO nanoparticles optical band-gap energy was determined using the following standard formula: $(\alpha h\upsilon)^m = k\,(h\upsilon\text{-}E_g)$ [18], where '$h\upsilon$' denotes the incident photon energy, 'k' is a constant, '$E_g$' is the optical band-gap energy, and 'm' is an exponent term that indicates the type of transition such as direct (m = 2), indirect (m = 1/2), direct forbidding (m = 2/3), and indirect forbidden transition (m = 1/3). This study solely took into account the direct transitions, or m = 2, for CZAFO samples. As the absorption coefficient $\alpha$ approaches zero, optical band-gap energies of the CZAFO nanoparticle were calculated by extrapolating a linear component of the curve in the direction of the X-axis. This was discovered by looking at plots of photon energy ($h\upsilon$) vs $(\alpha h\upsilon)^2$ (Figure 6). CZAFO nanoparticles were optical band gap energies ranging from 1.647 eV to 1.487 eV, depending on the composition (x = 0.2, 0.4, 0.6, and 0.8), hold promise for a sort of optoelectronic applications and including photocatalysis, optical sensors and biomedical imaging [11,17,18]. Also, optical band gap energy ($E_g$) values were provided to indicate the semiconductor nature of CZAFO nanoparticles.

## 4 Conclusion

In the present study, $Al^{3+}$ substituted $Co_{0.3}Zn_{0.7}Al_xFe_{2-x}O_4$ (x = 0.2, 0.4, 0.6, 0.8) / CZAFO nanoparticles compositions were successfully studied through the hydrothermal method. XRD pattern confirms the formation of a single-phase spinel structure without any impurities. The average crystallite size, lattice parameter, specific surface area and unit cell volume of the prepared ferrite were increased by increasing the $Al^{3+}$ content. The visible range of the samples was PL spectra showed that the emission peaks ranged from 360 to 615 nm, with a maximum detected at 475nm & 480nm. This electronic emission may be caused by radiative deficits at grain boundaries and oxygen vacancies inside the crystal structure. The FT-IR spectra of the

sample revealed the presence of ferrite, as evidenced by the main two absorption peaks in the region of 469 to 486 $cm^{-1}$ for $\upsilon_b$ (octahedral sites) and 434 to 447 $cm^{-1}$ for $\upsilon_a$ (tetrahedral sites). Optical energy band gap was also influenced by increasing the x-value with a decrease from 1.647 to 1.487 eV with increasing from x =0.2 to 0.8 for suitable applications of an optoelectronic, optical sensors, biomedical imaging and semiconductor nature.

## Acknowledgements

The researchers are grateful to Dr. M. V. Lakshmaiah, Professor of Physics and Electronics at Sri Krishnadevarya University in Ananthapuramu, for providing the research lab. Authors also thankful for the required characterizations (FTIR and UV-Vis) by SRMIST consulting, SRM University, Chennai. Yogi Vemana University, YSR Kadapa and IISc, Bangalore were acknowledged for the photoluminescence and X-ray diffraction characterizations respectively.

## References

1) Salih SJ, Mahmood WM. Review on magnetic spinel ferrite (MFe2O4) nanoparticles: From synthesis to application. *Heliyon*. 2023;9(6):1–25. Available from: https://doi.org/10.1016/j.heliyon.2023.e16601.
2) Nazir S. Mini Review: Synthesis and Applications of Spinel Ferrites (Mfe2o4). *Determ in Nanomed & Nanotech*. 2023;3(2):1–4. Available from: https://www.researchgate.net/publication/373049111_Mini_Review_Synthesis_and_Applications_of_Spinel_Ferrites_Mfe2O4.
3) Thakur P, Chahar D, Taneja S, Bhalla N, Thakur A. A review on MnZn ferrites: Synthesis, characterization and applications. *Ceramics International*. 2020;46(10):15740–15763. Available from: https://doi.org/10.1016/j.ceramint.2020.03.287.
4) Subbaiah DCV, Dastagiri S, Pakardin G, Prasad K, Ameena P, Supriya KE, et al. Investigations on structural and functional properties of Zinc Cobalt ferrite nanoparticles. *International Journal of Creative Research Thoughts*. 2024;12(2):787–798. Available from: https://www.ijcrt.org/papers/IJCRT2402679.pdf.
5) Andhare DD, Patade SR, Kounsalye JS, Jadhav KM. Effect of Zn doping on structural, magnetic and optical properties of cobalt ferrite nanoparticles synthesized via. Co-precipitation method. *Physica B: Condensed Matter*. 2020;583. Available from: https://doi.org/10.1016/j.physb.2020.412051.
6) Alhassan S, Alshammari AH, Alotibi S, Alshammari K, Mohamed WS, Hadia NMA. Structural and Optical Properties of Nickel-Doped Zinc Sulfide. *Nanomaterials*. 2019;14(19). Available from: https://doi.org/10.3390/nano14191599.
7) Alange RC. Alange (2021) Structural and Magnetic properties of Zn2+ doped Cobalt Ferrite Nanoparticles synthesized by Sol-gel Auto Combustion Method. *International Journal of Science and Research (IJSR)*. 2021;10(7):981–983. Available from: https://www.researchgate.net/publication/353571689_Structural_and_Magnetic_Properties_of_Zn2_Doped_Cobalt_Ferrite_Nanoparticles_Synthesized_by_Sol-gel_Auto_Combustion_Method.
8) Ali HT, Amin N, Akhtar M, Arshad MI, Athar MK, Morley NA, et al. Synthesis and characterizations of nickel doped Co-Zn-Y ferrites. *Journal of Ovonic Research*. 2023;19:65–72. Available from: https://chalcogen.ro/65_AliHT.pdf.
9) Gilani ZA, Farooq A, Asghar NUHK, Khalid M. Synthesis and Characterization of Lanthanum doped Co-Zn spinel ferrites nanoparticles by Sol-Gel Auto Combustion Method. *Journal of Materials and Physical Sciences*. 2020;1(1):1–11. Available from: https://journals.internationalrasd.org/index.php/jmps/article/view/590/326.
10) Rather SU, Lemine OM. Effect of Al doping in zinc ferrite nanoparticles and their structural and magnetic properties. *Journal of Alloys and Compounds*. 2020;812. Available from: https://doi.org/10.1016/j.jallcom.2019.152058.
11) Dastagiri S, Pakardin G, Babu TA, Lakshmaiah MV, Naidu KCB. Colossal dielectric behavior in Al0.8 Gdy La0.2-yTiO3 (y = 0.01-0.04) nanostructures. *Journal of Materials Science: Materials in Electronics*. 2021;32:8017–8032. Available from: https://www.researchgate.net/publication/349664927_Colossal_dielectric_behavior_in_Al08GdyLa02-yTiO3_y_001-004_nanostructures.
12) Das SB, Singh RK, Kumar V, Kumar N, Singh P, Naik NK. Structural, magnetic, optical and ferroelectric properties of Y3+ substituted cobalt ferrite nanomateraials prepared by a cost- effective sol-gel route. *Materials Science in Semiconductor Processing*. 2022;145. Available from: https://doi.org/10.1016/j.mssp.2022.106632.
13) Hjiri M, Alonizan NH, Althubayti MM, Alshammari S, Besbes H, Aida MS. Preparation and photoluminescence of NiFe2O4 nanoparticles. *Journal of Materials Science: Materials in Electronics*. 2019;30:15379–15387. Available from: https://link.springer.com/article/10.1007/s10854-019-01914-9.
14) Yousaf M, Nazir S, Akbar M, Akhtar MN, Noor A, Hu E, et al. Structural, magnetic, and electrical evaluations of rare earth Gd3+ doped in mixed Co-Mn spinel ferrite nanoparticles. *Ceramics International*. 2022;48(1):578–586. Available from: https://doi.org/10.1016/j.ceramint.2021.09.136.
15) Jyothish B, Jacob J. Al- doped Zinc ferrite nanoparticles: Preparation and evaluation of thermal, structural, morphological and anticancer properties. *Journal of Alloys and Compounds*. 2021;863. Available from: https://doi.org/10.1016/j.jallcom.2020.158352.
16) Sagar TV, Rao TS, Raghuram N. Temperature dependent structural, morphological, FTIR, optical, magnetic properties of NiMgZn ferrites. *Nanosystems Physics Chemistry Mathematics*. 2020;11(4):434–443. Available from: https://www.researchgate.net/publication/345922312_Temperature_dependent_structural_morphological_FTIR_optical_magnetic_properties_of_NiMgZn_ferrites.
17) Naresh U, Kumar RJ, Naidu KCB. Hydrothermal synthesis of barium copper ferrite nanoparticles: Nanofiber formation, optical, and magnetic properties. *Materials Chemistry and Physics*. 2019;236. Available from: https://doi.org/10.1016/j.matchemphys.2019.121807.
18) Jameel MH, Agam MA, Hamzah MQ, Roslan MS, Rizvi SZH, Yabagi JA. Structural, optical and morphological properties of zinc -doped cobalt-ferrites CoFe2−xZnxO4 (x=0.1-0.5). *Digest Journal of Nanomaterials and Biostructures*. 2021;16(2):399–408. Available from: https://openurl.ebsco.com/EPDB%3Agcd%3A14%3A25136494/detailv2?sid=ebsco%3Aplink%3Ascholar&id=ebsco%3Agcd%3A150479411&crl=c&link_origin=www.google.com.